Doppler Radar Observations of the Development of a Boundary-Layer Nocturnal Jet

A. SHELBY FRISCH, BRAD W. ORR, AND BROOKS E. MARTNER

NOAA/ERL/Wave Propagation Laboratory, Boulder, Colorado

(Manuscript received 27 September 1990, in final form 11 June 1991)

ABSTRACT

A single Doppler radar obtained detailed clear-air measurements of the development of a strong boundary-layer nocturnal jet in North Dakota during the summer of 1989. The evolution of the jet was monitored by the radar with a high degree of vertical and temporal resolution using a repetitive sequence of four different elevation scans. A new variation of the velocity–azimuth display (VAD) analysis technique provided vertical profiles of the mean wind components and several turbulence terms. Boundary-layer wind speeds began to increase in the late afternoon, well before sunset, as surface cooling began. Wind speeds accelerated faster after sunset and eventually produced a jet that exceeded 23 m s^{-1} at about 0.5 km AGL. The wind veered with height and time and followed the expected inertial oscillation pattern. Measured shear stresses, vertical fluxes of momentum, and velocity variances, which were initially large, decreased sharply after the surface began to cool. The directly measured vertical velocities were significantly downward during the late afternoon and upward at night.

1. Introduction

The low-level nocturnal jet is a common phenomenon in various parts of the world and is particularly prevalent in the central United States. Some studies suggest that it is an important ingredient in the initiation of thunderstorms (Bonner 1966; Raymond 1978; Uccellini and Johnson 1979) and mesoscale convective complexes (Maddox 1983). It also has implications for aviation (Blackadar 1957), agricultural and air pollution meteorology, and wind energy (McNider and Pielke 1981). In a climatological analysis of National Weather Service (NWS) radiosonde data, Bonner (1968) found that these jets occur from Canada to the Gulf of Mexico, and the maximum frequency of occurrence is over Oklahoma and Kansas. The vast majority of low-level jets he studied exhibited southerly flow; summer was the season of greatest frequency of occurrence.

Blackadar (1957) noted that the wind-speed maximum is frequently observed at night below 1 km, and the maximum speed is usually located at the top of the nocturnal inversion. This maximum is often supergeostrophic, and very strong wind shear is associated with it. He proposed that the supergeostrophic wind is due to an inertial oscillation triggered by the loss of the daytime mixing frictional restraint and the initiation of an inversion at sunset. Holton (1967) modeled the dynamics of the boundary layer and showed that diurnal variations of heating and cooling on sloping terrain could account for the amplitude of jets observed over the Great Plains. Together, the diurnal oscillation of frictional forces and the diurnal differential heating of sloping terrain can account for most of the general characteristics of observed nocturnal jets.

Using combined profile and turbulent exchange coefficient formulations for the unstable and stable boundary layers, McNider and Pielke (1981) modeled the full diurnal boundary-layer cycle on a coarse mesoscale grid. When applied to sloping terrain approximating the Great Plains, the model showed that generation of pressure gradients caused by elevated terrain heating and cooling is a dominant factor in the evolution of the diurnal wind structure. Fast and McCorcle (1990), using a two-dimensional model, examined the sensitivity of nocturnal jets to additional features, such as thermal and frictional perturbations and variations of slope, latitude, soil type, and soil moisture content.

In a case study of the low-level jet, Parish et al. (1988) made airborne altimeter measurements of the geostrophic wind at different levels over Oklahoma. The measurements helped confirm previous theoretical and numerical studies showing the importance of the diurnal heating cycle over sloping terrain in producing an oscillating, horizontal, pressure gradient force. They also documented the inertial turning of the jet as a result of frictional decoupling and concluded that the diurnal variation of frictional forces was the dominant mechanism forcing the jet they observed. Lenschow et al. (1988) probed another nocturnal jet by aircraft.

It is evident that previous investigations of nocturnal jets have primarily relied on numerical modeling and

Corresponding author address: Dr. A. Shelby Frisch, NOAA Wave Propagation Laboratory, 325 Broadway, Boulder, CO 80303.

in situ measurements by balloon soundings. In this study, we demonstrate how a remote-sensing technique can provide nearly continuous, high-resolution measurements of a nocturnal jet, and we use the technique to extend the limited body of observations on this phenomenon.

Doppler radar has been used extensively in a research mode to examine airflow patterns in precipitation and clear air. Its capacity to provide continuous measurements of wind and turbulence make it another promising candidate for examining boundary-layer jets. Lhermitte (1966) and Stensrud et al. (1990) also reported the detection of nocturnal jets by Doppler radar. The present study, however, is the first to also examine radar measurements of boundary-layer turbulence features associated with a nocturnal jet.

More observations of nocturnal jets can be expected soon, when the clear-air Doppler radar wind profilers of the NOAA Profiler Demonstration Network (Chadwick and Hassel 1987) begin continuous operation across the central United States. However, the lowest measurement level (500 m) for these profilers will be above many low-level jets, and the vertical resolution will be rather coarse (250 m). The higher-frequency wind-profiling radar described by Ecklund et al. (1988) is better suited for the study of boundary-layer jets, and some variation of that system may eventually accompany the operational network of profilers. However, neither of these types of fixed-beam profilers can match the vertical resolution, velocity, and turbulence measurement precision of the scanning Doppler radar measurements described in this study. NEXRAD Doppler weather radars that will also soon become operational should be able, if scanned appropriately, to provide nocturnal jet measurements with resolutions similar to those reported here. Stensrud et al. (1990) examined the mean wind speeds in a nocturnal jet from measurements using a NEXRAD prototype.

2. The Doppler radar technique

Although designed primarily for measuring precipitation, the NOAA Wave Propagation Laboratory's X-band (3.2-cm wavelength) Doppler radars also have sufficient sensitivity to detect natural scatterers in the clear air of the planetary boundary layer. These scatterers are believed to be dust, seeds, small insects, and other particles of 1 mm and smaller (Kropfli 1986). During the warmer months over continental locations, these scatterers are normally present in abundance in the clear air, and the radar is able to measure their velocities (which are assumed to trace the air motions) and map the airflow patterns within a few kilometers of the radar and to the top of the boundary layer or slightly higher.

Using the conical scanning procedure described below, the radar can measure the mean wind and other moments of the velocity spectra as a function of height with good vertical and temporal resolution. Various wind and turbulence statistics such as the vertical flux of momentum, momentum-flux production terms, and vertical flux of turbulent kinetic energy can be computed from these measurements. Unlike balloon soundings, the radar measurements can be virtually continuous, and unlike aircraft, the radar provides simultaneous measurements at many heights. Thus, the Doppler radar is a very suitable instrument for studying low-level jets and examining how their behavior is related to turbulence quantities.

The scanning and analysis methods used to determine wind profiles and stress components are referred to as velocity–azimuth display (VAD) techniques. These have been reviewed by Kropfli (1986) for Doppler radar measurements and for Doppler lidar by Eberhard et al. (1989). Browning and Wexler (1968) developed this method to measure the speed and direction of the mean wind at a fixed height above the ground by scanning the radar at a constant elevation angle. By fitting a Fourier series to the measured radial velocities as a function of azimuth at a fixed range, they related the first-harmonic coefficients to the mean speed and direction. Using the same conical scan, Wilson (1970) measured several second-moment quantities. He found that by computing the variance of the Doppler velocity around the scan circle, he could compute $\overline{u'v'}$, $\overline{u'w'}$, $\overline{v'w'}$, $\overline{u'^2 + v'^2}$, and $\overline{w'^2}$, where u, v, and w are defined in the conventional sense. The primes indicate perturbations or deviations from the mean, and the overbars denote a spatial average. This computation required assuming the perturbation quantities were horizontally homogeneous across the scan circle. To ensure that the assumption of horizontal homogeneity was more fully satisfied, and to expand the range of horizontal scales included in the estimates, Kropfli (1986) extended Wilson's analysis by averaging several scans taken during periods of 20 min or longer. In this study we assume that horizontal homogeneity applied, and employ the averaging technique of Kropfli (1986) with new computational methods described by Frisch (1991). The procedure is reviewed below.

Figure 1 shows the scanning geometry and Fig. 2 shows a sample of the radial-velocity measurements obtained from a single scan of the NOAA X-band Doppler radar. Browning and Wexler (1968) showed that the relationship between the measured radial velocity V_R, and the mean wind at fixed range r, elevation angle θ, and azimuth β, at scan time t, is given by

$$V_R(\beta, \theta, t) = u(\beta, \theta, t)\sin(\beta)\cos(\theta) + v(\beta, \theta, t)\cos(\beta)\cos(\theta) + w(\beta, \theta, t)\sin(\theta). \quad (1)$$

Assuming linear variations of the mean wind across the scan circle, the mean speed and direction are determined from the measurements of V_R by expanding the horizontal wind fields in terms of mean components u_0, v_0, and w_0 and gradients as

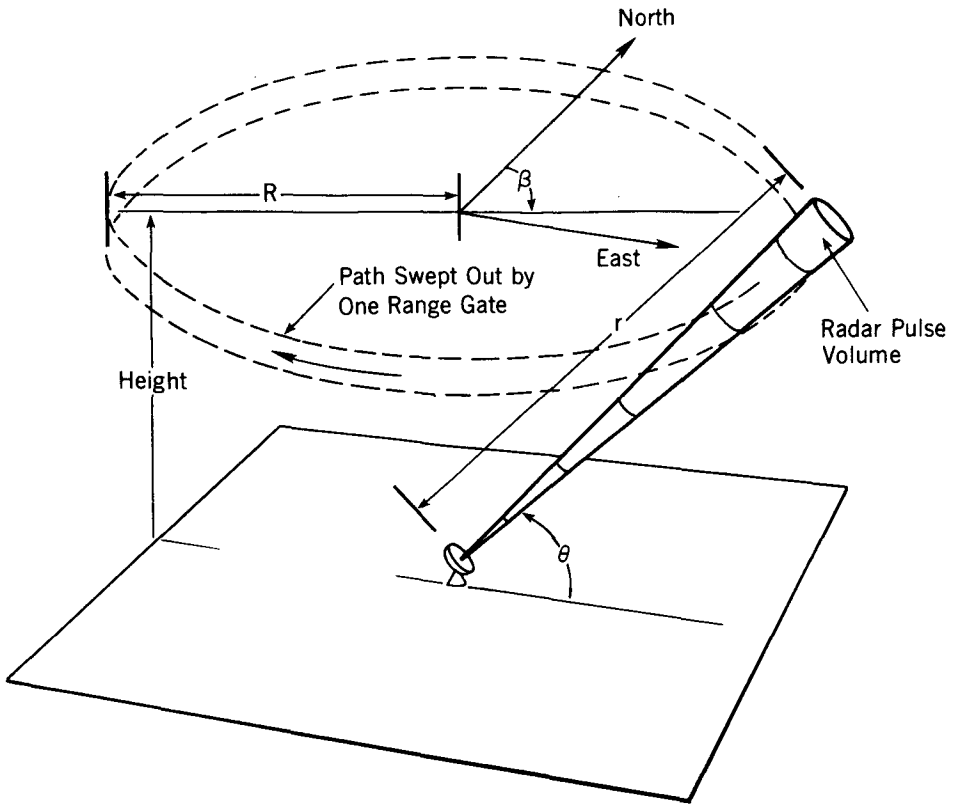

FIG. 1. Schematic drawing of the scanning geometry.

$$u = u_0 + x\left(\frac{\partial u}{\partial x}\right) + y\left(\frac{\partial u}{\partial y}\right) \quad (2a)$$

$$v = v_0 + x\left(\frac{\partial v}{\partial x}\right) + y\left(\frac{\partial v}{\partial y}\right) \quad (2b)$$

$$w = w_0. \quad (2c)$$

Substituting Eqs. (2a)–(2c) into Eq. (1) yields a complicated equation with the general form of a Fourier series

$$\overline{V_R(\beta, \theta, t)} = a_{0t} + a_{1t}\sin(\beta) + a_{2t}\cos(\beta) + a_{3t}\sin(2\beta) + a_{4t}\cos(2\beta), \quad (3)$$

where the overbar represents an average over an entire revolution that is assigned a unique time t. Temporal averaging can then be applied to numerous revolutions at the same elevation angle and range. Values of the coefficients are yielded by Fourier analysis of the data. The mean wind components are related to the coefficients by

$$u_0 = a_{1t}/\cos(\theta) \quad (4a)$$

$$v_0 = a_{2t}/\cos(\theta), \quad (4b)$$

and for large θ,

$$w_0 = a_{0t}/\sin(\theta). \quad (4c)$$

The assumption of linearity of the mean wind can be checked by comparing the mean winds computed from the data of different elevation scans. This was done for the present study using measurements from three different elevation angles, ranging from 35° to 69°. The differences were found to be very small, thus validating the linearity assumption in this case.

The second moment of the measured radial velocity can be related to second moments of the wind field by using Eq. (1). This gives the following relationship for the variance of the radial velocity:

$$\begin{aligned}\mathrm{var}(V_R) &= \overline{(V_R - \bar{V}_R)^2} \\ &= \overline{u'^2}\cos^2\theta\sin^2\beta + \overline{v'^2}\cos^2\theta\cos^2\beta + \overline{w'^2}\sin^2\theta \\ &\quad + \overline{u'v'}\cos^2\theta\sin 2\beta + \overline{u'w'}\sin 2\theta\sin\beta \\ &\quad + \overline{v'w'}\sin 2\theta\cos\beta. \end{aligned} \quad (5)$$

Wilson (1970) solved for the momentum fluxes of Eq. (5) by integrating the variance over four azimuth quadrants of the scanned circle. Kropfli (1986), Frisch et al. (1989), and others have also used this approach. In this study, however, we use a newer procedure in-

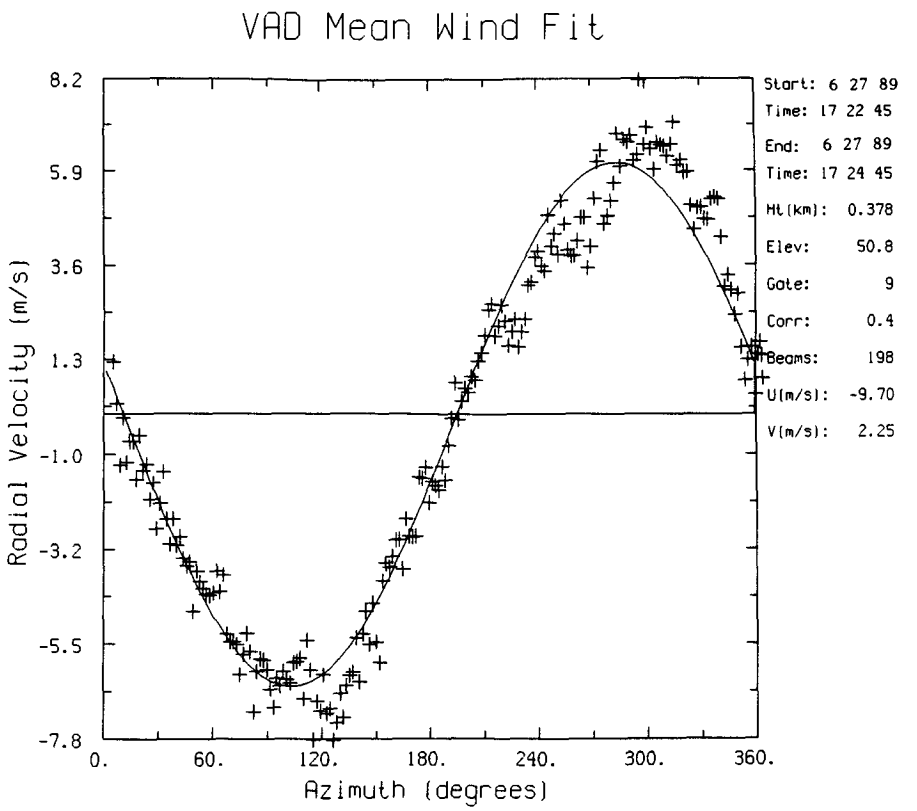

FIG. 2. Sample of Doppler velocity data from a single scan on 27 June 1989 for 378 m AGL. Measurements for 197 beams are shown as points; the smooth solid line is a sinusoidal fit to the data.

troduced by Frisch (1990). He expanded each flux term of Eq. (5) in terms of a mean and horizontal gradient and conducted a Fourier analysis of both sides of the equation. This is analogous to the analysis Browning and Wexler (1968) applied to Eq. (1). It allows data of the entire scan to be incorporated in one calculation and provides more uniform weighting around the scan circle than does Wilson's method.

Frisch (1990) also derived a complex solution for the more general case that allows horizontal gradients of the perturbation wind quantities. However, to simplify the computational effort for the measurements discussed here, we have resorted to the conventional assumption of horizontal homogeneity of the perturbation quantities. As a check of this assumption, we compared momentum-flux calculations from the 35° and 51° elevation-angle scans. The absolute value of the fluxes differed by only about 20% and the vertical gradients of the fluxes differed even less.

3. Scanning strategy and specifications

The boundary-layer jet measurements described in this study were obtained near New Salem, North Dakota, during the North Dakota Thunderstorm Project (NDTP) of 1989. Locally the terrain contains scattered small hills, but statewide it is fairly flat and slopes upward from east-northeast to west-southwest by about 0.007°. A Wave Propagation Laboratory (WPL) X-band Doppler radar was programmed to conduct a continuous series of conical scans starting in the afternoon on clear days when storms were not within radar range. In the evening it was left to continue the scans unattended until the data tapes ran out after midnight. The scan sequence used four different elevation angles. Each scan required 2 min; then the elevation was incremented until all four elevation angles were covered and the sequence was repeated. Thus, the total time for all four elevations angles (one complete volume scan) was 8 min.

As shown by Frisch et al. (1989), at certain elevation angles the analysis equations simplify to yield direct measurements of various turbulence quantities. With this in mind, the four elevation angles were chosen to be 35.3°, 50.8°, 68.9°, and 89.9°. The mean wind components ($\underline{u}$, $\underline{v}$, $\underline{w}$) and vertical flux of horizontal momentum ($\overline{u'w'}$, $\overline{v'w'}$) can be computed from any of the first three elevations. The turbulent kinetic energy

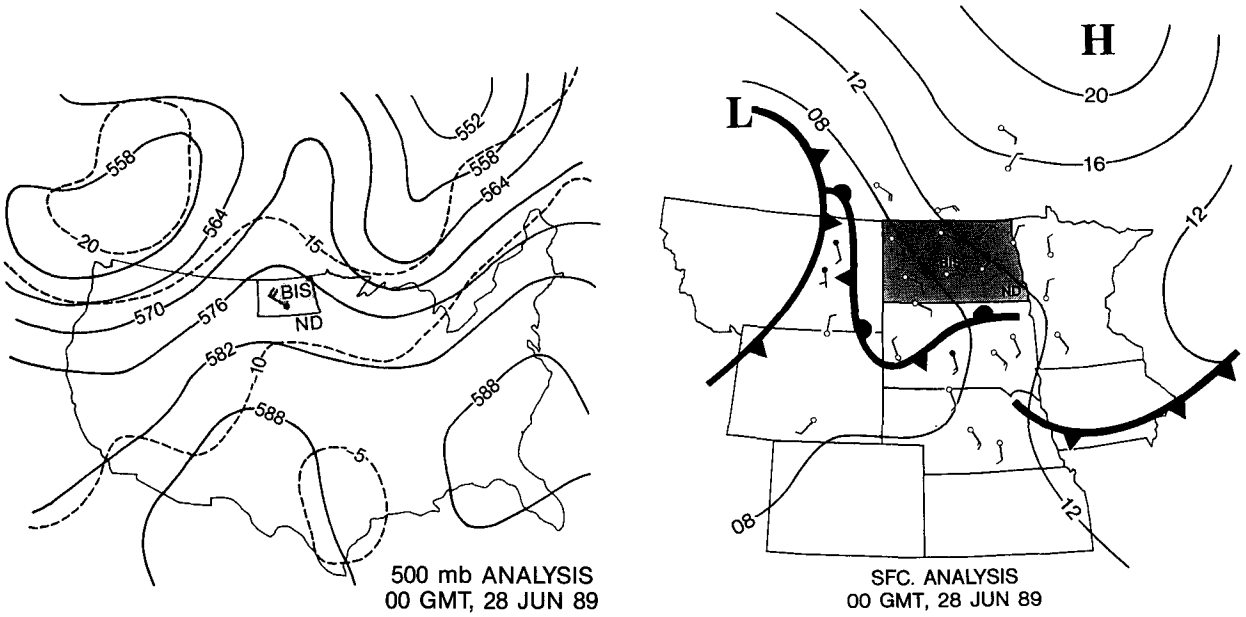

FIG. 3. (a) 500-mb map and (b) surface weather map for 1900 CDT 27 June 1989 (0000 UTC 28 June 1989).

$(\overline{u'^2 + v'^2 + w'^2})$ can be computed from the 35.3° scan and its vertical flux is obtained from the 50.8° elevation. Variance of the vertical velocity $\overline{w'^2}$ is obtained by Fourier analysis of data from the 89.9° scan.[1] This scan is also used for direct measurement of w.

The 50.8° scan was selected for computation of the mean wind and vertical flux of turbulent momentum terms in this study. This is near the 45° optimum angle for momentum-flux measurements (Kropfli 1986) and represents a compromise between maximizing the radar height coverage and minimizing wind velocity measurement errors. The range gate spacing was 75 m, which translates to a height resolution of 58 m at the 50.8° elevation angle.

At each range gate, 255 pairs of pulses were electronically averaged in 0.4-s dwell time to estimate the radial velocity. A total of 197 beams (azimuths around the scan circle) were included in each constant elevation sweep. Thus, every 2 min, 197 samples of velocity were obtained at each measurement height. About eight volume scans, each containing four elevation angles, were collected every hour. A quality criterion was imposed on the Doppler velocity data at each range gate to prevent very weak signals from being included in the hourly averages. It required that the data from at least 50 of the 197 beams exceed a specified signal detection threshold for all eight scans during the hour.

The data collection and processing represent a very substantial amount of sampling and result in a high degree of precision in the wind estimations. Using a similar number of beams, Kropfli (1986) compared estimates made by two collocated radars scanning at the same elevation angle and obtained an estimate of about 0.1 m s^{-1} for the precision of the measurements.

The largest scales or turbulence wavelengths sampled in the harmonic analysis of these measurements depend on the radar-pulse volume size and the maximum distance the air traveled during a revolution of the antenna. For the case of a narrow beam (0.8°) and short sampling ranges in the boundary layer, the largest dimension of the pulse volume is the pulse length, which was about 100 m. Assuming a typical wind speed of 10 m s^{-1} and using the 2-min scan time yields a maximum wavelength of 1.2 km.

4. Meteorological conditions

A strong boundary-layer jet was observed by the radar on 27–28 June 1989 during the NDTP. The case was characterized by weak dynamics at upper levels. An upper-level pressure ridge was located over the project area and produced fairly light winds above the boundary layer. At the surface, however, a very shallow area of low pressure in eastern Montana and high pressure in southern Manitoba created a strong pressure gradient across North Dakota. No fronts passed the radar during the data collection period of 1626–0224 CDT[2] (2126 UTC 27 June–0724 UTC 28 June). The afternoon was clear and hot, followed by rapid radiational cooling at night. The high temperature recorded

[1] Due to limitations of the antenna controller software, the 90.0° elevation was not available. The slight difference from true zenith pointing has negligible effects on the resulting measurements.

[2] Central daylight time, CDT = UTC − 5 h.

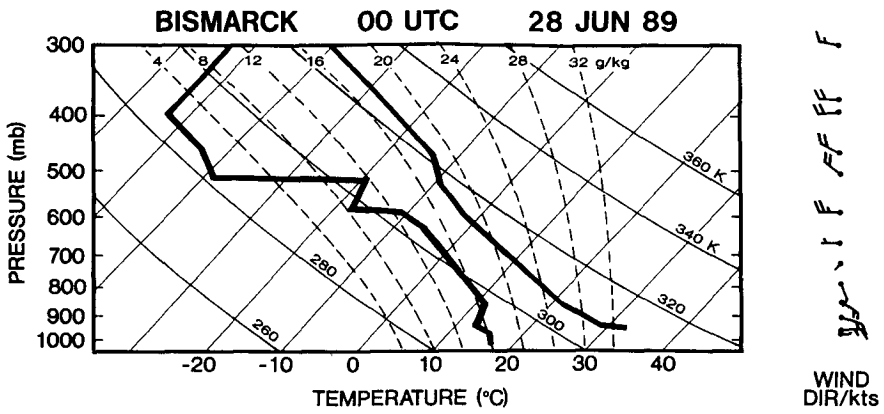

FIG. 4. Sounding from radiosonde launch from Bismarck, ND, at 1900 CDT 27 June 1989 (0000 UTC 28 June 1989).

in Bismarck by the NWS on the afternoon of 27 June was 33°C at 1650 CDT; a low of 14°C was reached 12 h later. Sunset occurred at 2135 CDT.

A corresponding surface-analysis map shown in Fig. 3b reveals the strong pressure gradient and easterly flow that prevailed across most of North Dakota. This surface gradient intensified during the observational period, as the high pressure strengthened in Manitoba and Minnesota and the low pressure area extended into western South Dakota. The intensification was more

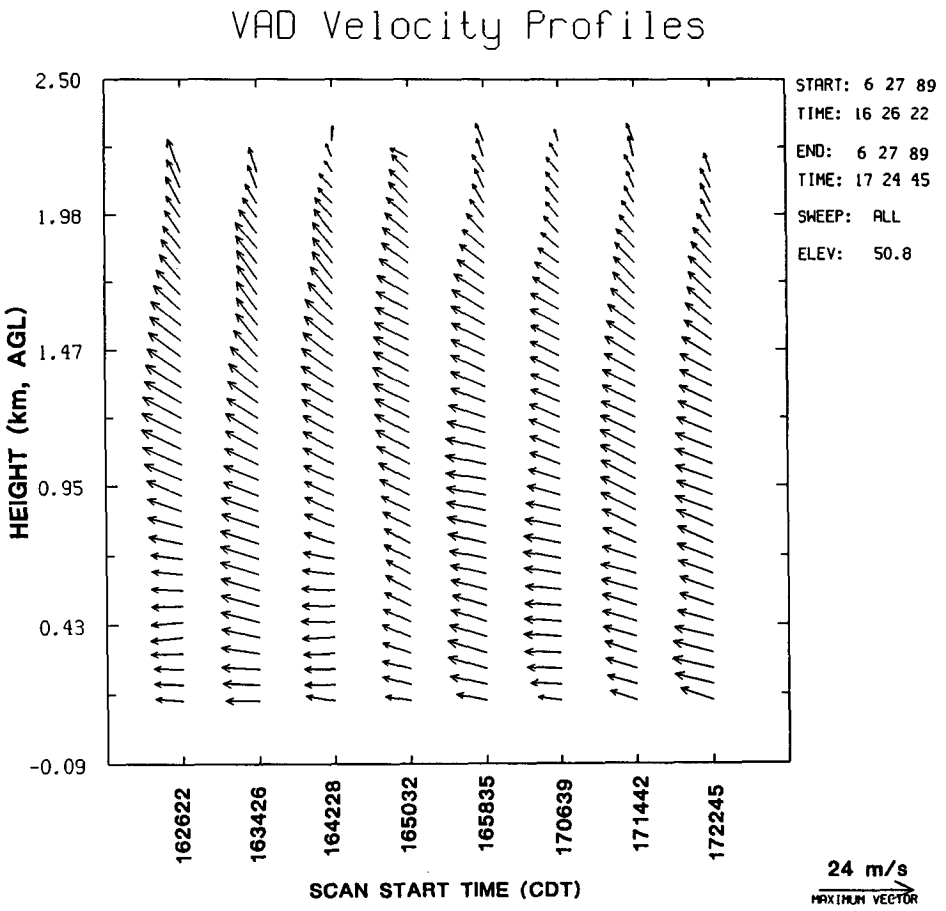

FIG. 5. Profiles of horizontal wind vectors shown at 8-min intervals for (a) 1624–1728 CDT and (b) 2146–2251 CDT. An arrow directed to the left represents a wind from the east.

pronounced in eastern North Dakota than near the radar, 50 km west of Bismarck, where the gradient began and remained strong during the radar measurements. The role of the low-level pressure gradient force in the jet's development is evaluated in section 6.

Winds veered with height on this afternoon and night. Figure 3a depicts the 500-mb map for 1900 CDT 27 June (0000 UTC 28 June) and shows a ridge located over North Dakota and northwesterly winds at Bismarck. At 700 and 850 mb (not shown) the winds over the northern Great Plains were from the southwest and south, respectively, and advected warmer air into the project area above the boundary layer.

Figure 3b also shows that a stationary front was aligned approximately east–west across the northern part of South Dakota. Convergence along this front helped initiate strong thunderstorms in this region of South Dakota. The project surveillance Doppler radar located in Bismarck detected a gust front that spread northward from the storms, but it dissipated 45 km south of the WPL radar. Thus, the VAD measurements collected by the WPL radar were apparently unaffected by the distant thunderstorms.

The 1900 CDT NWS radiosonde data from Bismarck are plotted in Fig. 4. The sounding shows a weak low-level jet of 9 m s^{-1} from the east-southeast at this time. Westerly flow prevailed above 3 km. A surface-based radiational inversion had not yet formed and the almost uniform profiles of mixing ratio and potential temperature suggest that near-neutral stability and fairly well-mixed conditions were still in force in the lower atmosphere.

As shown in section 5, the WPL radar documented the development of a very strong boundary-layer jet of southeasterly flow on this evening. The following afternoon, several severe thunderstorms erupted in the project area. Boe and Johnson (1990) present evidence that the nocturnal jet contributed significantly to destabilization and to the formation of those storms.

5. Radar measurements of the jet

Figure 5a displays profiles of the horizontal vector wind at 8-min intervals using data of the 50.8° elevation scans. The period covered is 1626–1730 CDT, which was just after the maximum surface temperature

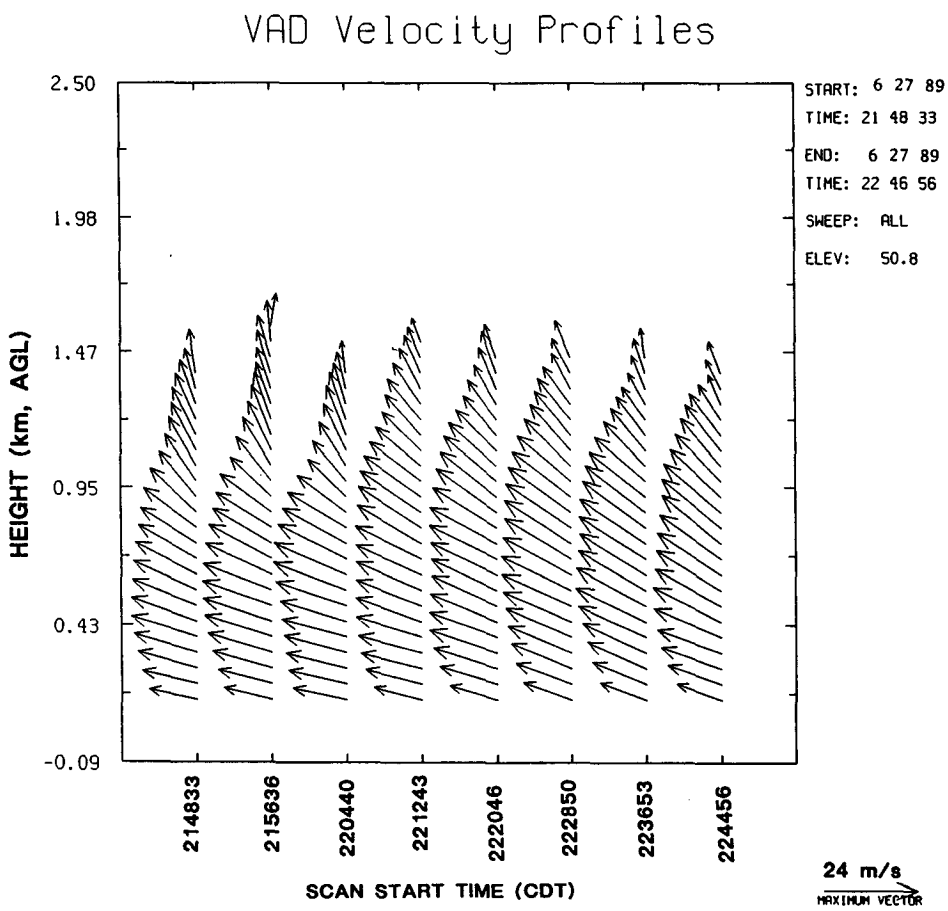

FIG. 5. (*Continued*)

was reached. The diagram reveals that the wind speeds and directions were quite uniform with height, as would be expected in a well-mixed convective boundary layer. The winds were from the east-southeast at about 8 m s^{-1}. Figure 5b shows the situation about 5 h later, at 2148–2253 CDT, just after sunset. By that time, the echo top had descended to about 1.5 km AGL and a prominent jet from the southeast had developed in about the middle of the echo layer. The strongest wind speed of 20 m s^{-1} was located ~0.5 km above the surface.

The evolution of the jet over a 10-h period is illustrated in the data presented in Figs. 6–10. Ten graphs are shown in each of these figures; each graph represents a 1-h average of the measurements except for the final graph, which is an average of the last 20 min of recorded data.

Figure 6 presents hourly averages of the mean wind speed measured with the 50.8° elevation scans. At the earliest time period (1626–1725 CDT), the wind speed was almost uniform with height over the 2-km depth shown. This occurred at the time of maximum surface temperature and is indicative of a well-mixed convective boundary layer. As time proceeded, the top of the radar echo descended from over 2 km at the start to about 1.5 km 10 h later in response to a shrinking boundary layer and weakening convective motions. The low-level jet developed a speed maximum shortly after the surface temperatures began to decline, but the development intensified after sunset to produce an average wind speed of almost 25 m s^{-1} at 0.5 km AGL during the final measurement period (0206–0224 CDT).

Boe and Johnson (1990) also detected the jet using data from a Doppler acoustic sounder in Bismarck, which provided wind measurements up to about 600 m AGL. Their limited profiles are similar to the radar profiles until 0100 CDT, after which time their indicated speeds (up to 40 m s^{-1} at 500 m AGL) became much stronger than those measured by the radar. Their data show the jet persisted until about 0600 CDT. It is not known whether the difference represents a measurement system problem or a true gradient of wind speed across the 50-km distance between the radar and the acoustic sounder. It is clear, however, that both systems detected a strong nocturnal jet over the NDTP area.

The development of the jet can also be traced in the hodographs of Fig. 7. This figure shows how the easterly and southerly components intensified with time. The southerly component, initially weaker, exceeded the easterly component at most heights after midnight. Thus, the wind vector rotated clockwise in a manner consistent with inertial turning.

Hourly averages of the mean vertical component of the wind based on the 89.9° elevation measurements are shown in Fig. 8. It shows that the mean vertical wind was negative in the lowest 1.5 km at the two earliest periods in the afternoon. Then, as surface cooling continued and convective motions relaxed, the vertical winds were close to zero at all heights. By the time of the last two profiles, however, the mean vertical

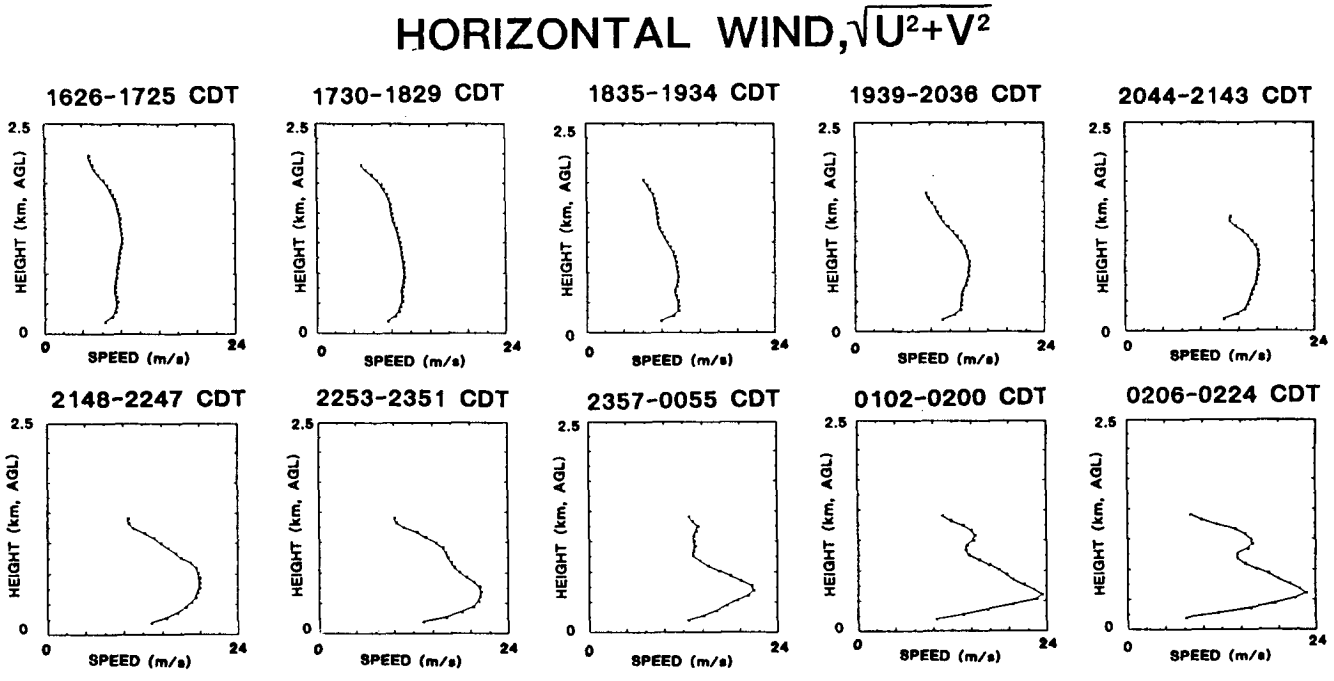

FIG. 6. Hourly average profiles of wind speed from the 50.8° elevation scans.

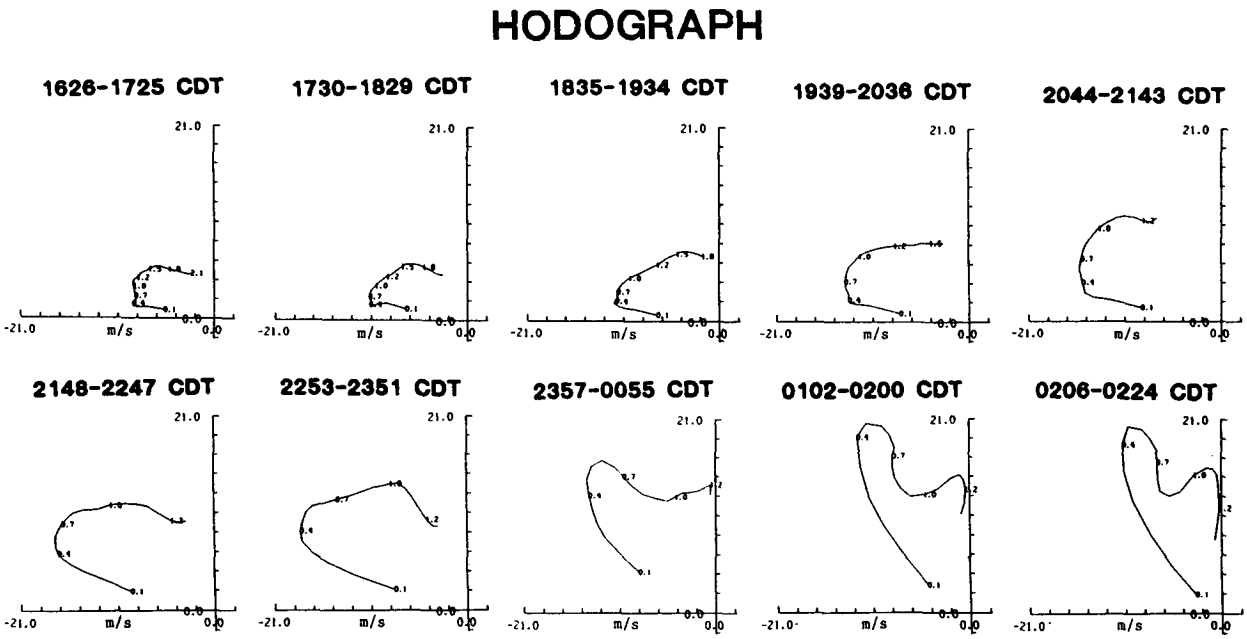

FIG. 7. Hodographs of hourly average winds from the 50.8° scans.

wind had become positive at all heights with a maximum value of about 0.5 m s^{-1} near 0.5 km AGL, approximately the jet height.

Hourly average profiles of the momentum flux or stress terms measured at the 50.8° elevation angle are portrayed in Fig. 9. Both stress terms were moderately large at most heights during the first 2 h, but became near zero around 1830 CDT and remained small thereafter. Figure 10 shows that the variance of vertical velocity measured with the 89.9° scans also decreased markedly after 1830. Large values in the lowest kilometer became much smaller as convection weakened

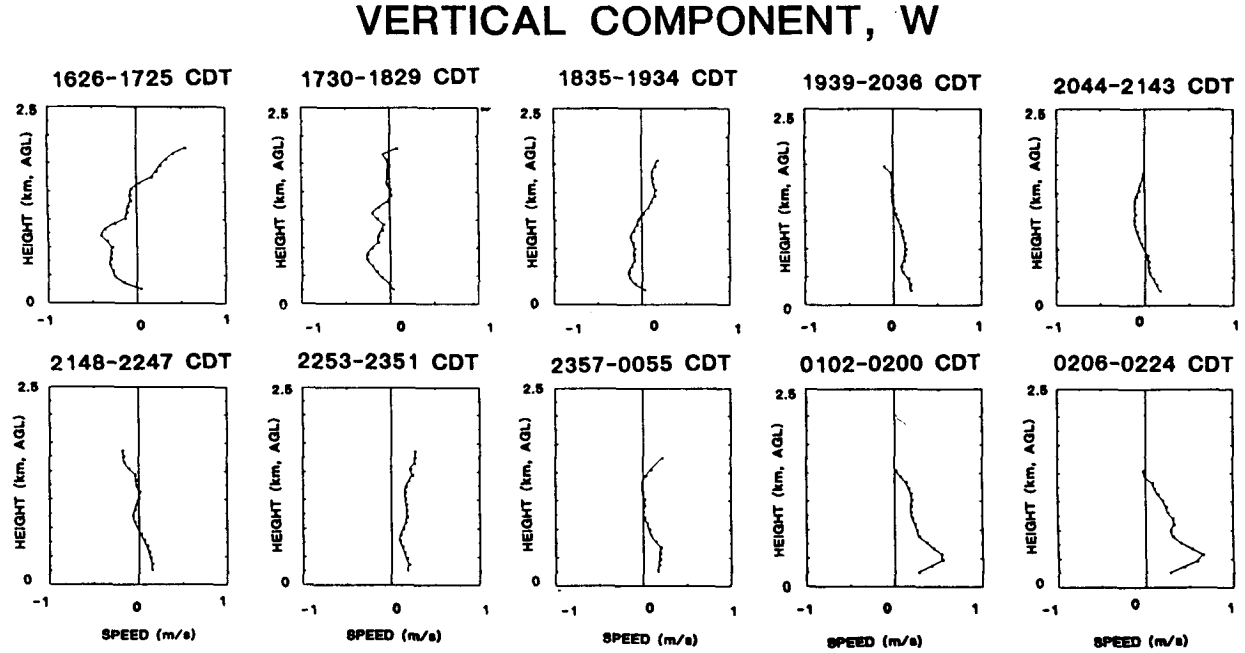

FIG. 8. Hourly average profiles of vertical wind velocity from the 89.9° scans.

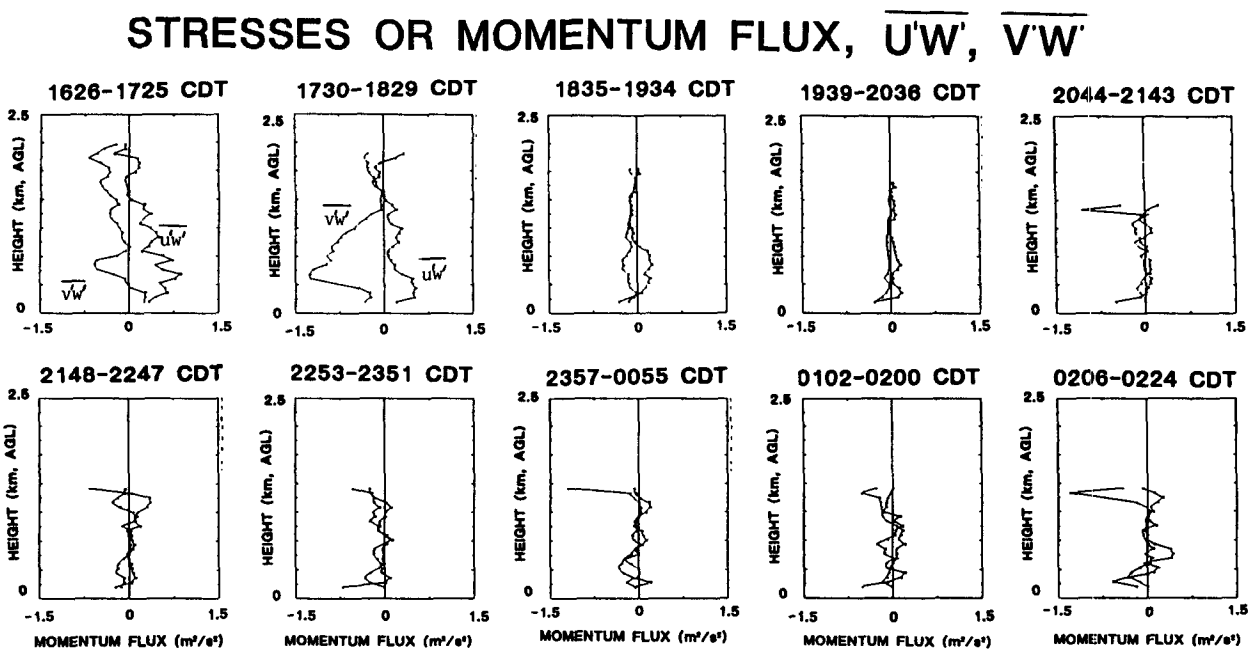

FIG. 9. Hourly average profiles of momentum stress terms from the 50.8° scans.

in response to cooling at the surface. This was also the time when the jet began to appear in the horizontal wind data.

Time series plots in Figs. 11 and 12 show the evolution of the hourly average wind at four different heights. Figure 11 reveals an intensification of both the u and v components beginning shortly after the time of maximum surface temperature. The v component generally increased at a steady rate until the final measurement period, when it began to decline at all four levels. In contrast, a time lag is found for the u component that reached its strongest value at the uppermost

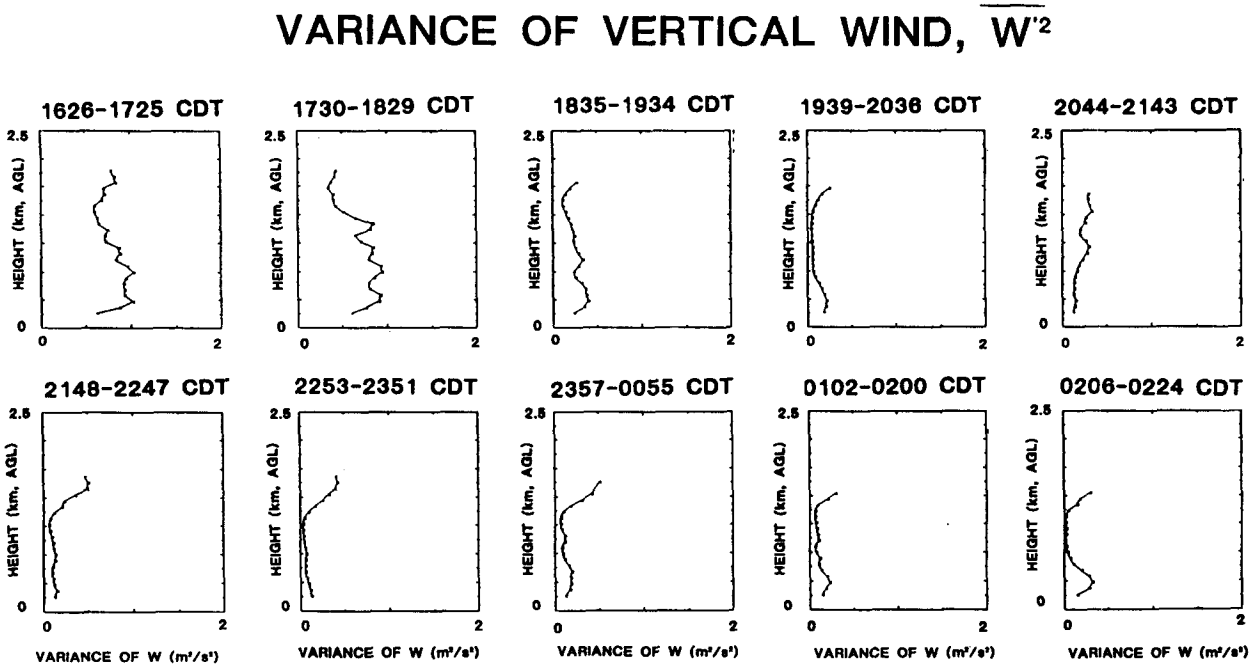

FIG. 10. Hourly average profiles of the variance of vertical velocity from the 89.9° scans.

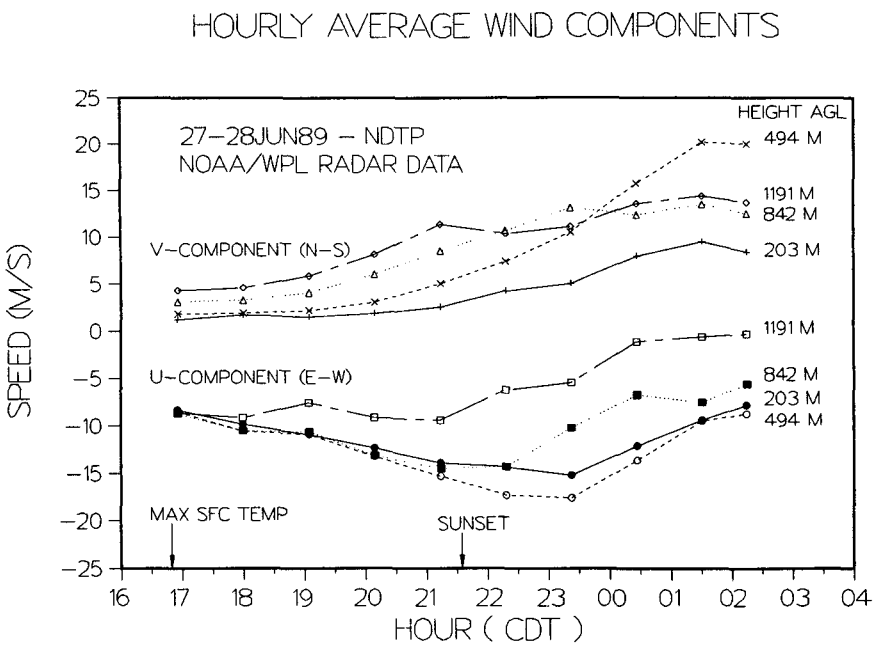

FIG. 11. Time series graph of the hourly average u and v wind components at four heights.

height just before sunset, and 1–2 h later at the lower heights. Its magnitude then steadily decreased at each height. Figure 12 shows that the wind directions changed slightly faster at the higher altitudes, with an acceleration of the veering occurring at all heights after sunset. The accelerated veering occurred first at the upper levels and later at the lower levels. The results are similar to those found by Lenschow et al. (1988), and agree with the concept that frictional restraints on the flow are released in sequence from the top of the boundary layer downward after surface cooling commences.

These features can also be seen in the hodograph format presentation of Fig. 13. In this figure, the veering

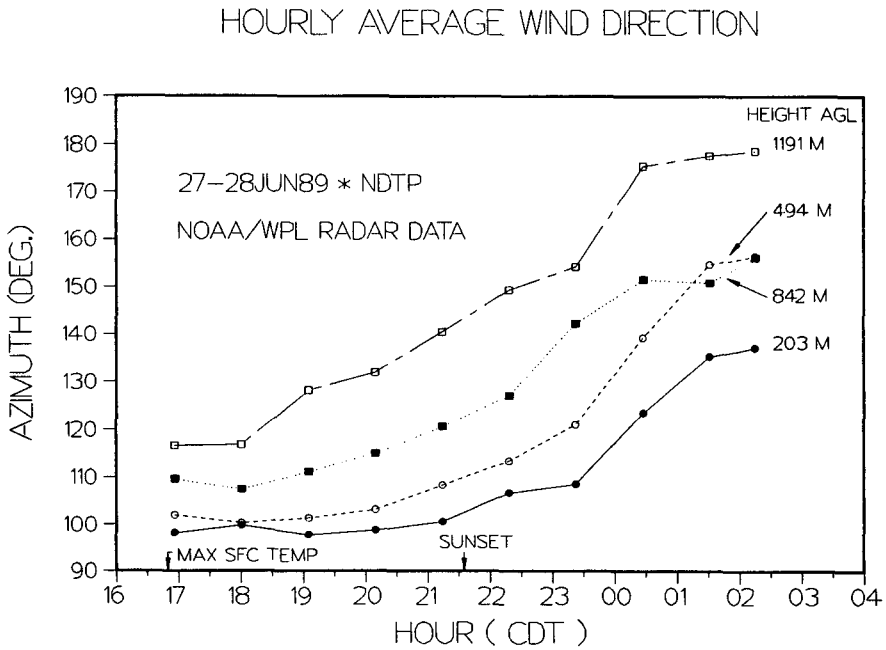

FIG. 12. Time series graph of hourly average wind direction at four heights.

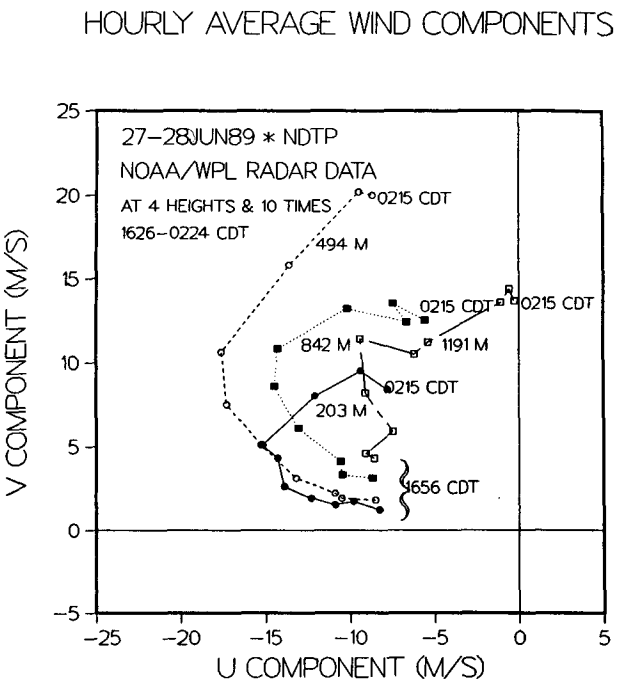

FIG. 13. Temporal progression of hourly average wind vector at four heights. Time increases in the clockwise direction along each curve.

of the wind at each height is apparent. Almost half of an ellipse was traced during the 10-h observation period. The data resemble the aircraft measurements of Parish et al. (1988), but the jet was weaker in their case. For the simple situation of purely inertial wind changes, Blackadar (1957) showed that the geostrophic wind vector is given by the center of the inertial oscillation ellipse in diagrams such as Fig. 13. There is evidence that this case, however, was not one of inertial changes alone.

Figure 14 summarizes the jet's development in a time–height presentation of wind speed constructed from the hourly average profiles. It is interesting to note that the speeds began to increase shortly after the maximum surface temperature was reached. This was well before sunset, which is the time most studies have regarded as the onset time for these jets. Near the end of the data collection period the average wind profiles showed a speed maximum of 23.4 m s^{-1} and a corresponding shear of almost 0.05 s^{-1} across the lowest 0.5-km depth of the atmosphere. A wave with a period of about 4 h is also prominent in the isotach pattern of Fig. 14 above the jet.

6. Discussion

The radar measurements show that as surface cooling began in the late afternoon, the Reynolds stresses or turbulent fluxes of momentum and the variance of vertical velocity quickly decreased to near zero values, and the jet began to appear. Lower-momentum air, slowed by frictional drag near the surface, was then no longer being strongly mixed with and retarding the airflow above it in the boundary layer. As cooling continued after sunset, the turbulent fluxes remained very small and the jet intensified as it veered with time. These radar observations are consistent with Blackadar's (1957) inertial oscillation explanation for the formation of strong nocturnal jets.

While the radar turbulence measurements leave little doubt that frictional decoupling encouraged the development of the jet, the contribution by the pressure gradient force is more difficult to evaluate from the available data. This is because the pressure gradient in the boundary layer is not known for this case, unlike the study reported by Parish et al. (1988) where it was measured by aircraft. At the surface, however, the pressure gradient was known to be strong and changing, as discussed in section 4. This suggests that temporal changes of the pressure gradient force may also have been significant in the boundary layer.

Figure 15 shows how the surface geostrophic winds changed in relation to the radar-observed wind-speed changes at the jet level. The surface geostrophic winds were determined in two ways. In one method, they were computed simply from the difference of station pressures reported at Dickinson (105 km west of the radar) and Grand Forks (450 km northeast of the radar). The selection of this particular pair of stations, however, biases the result toward the conditions in eastern North Dakota. The second method computed

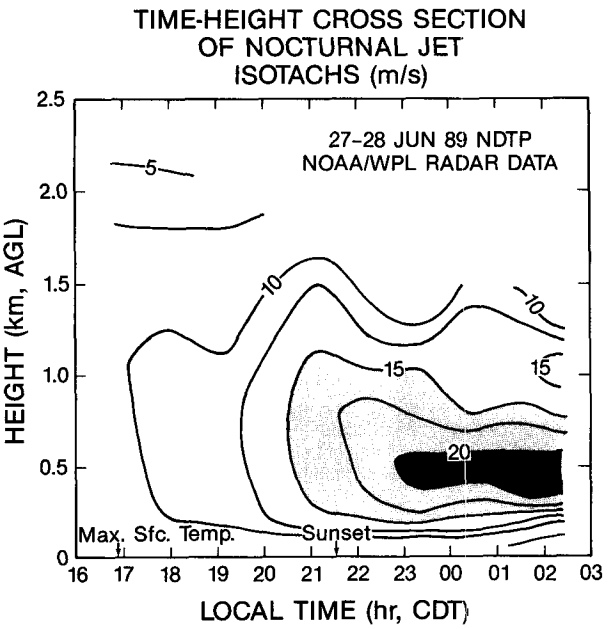

FIG. 14. Time–height cross section of wind speed constructed from the hourly average wind profiles measured by the radar.

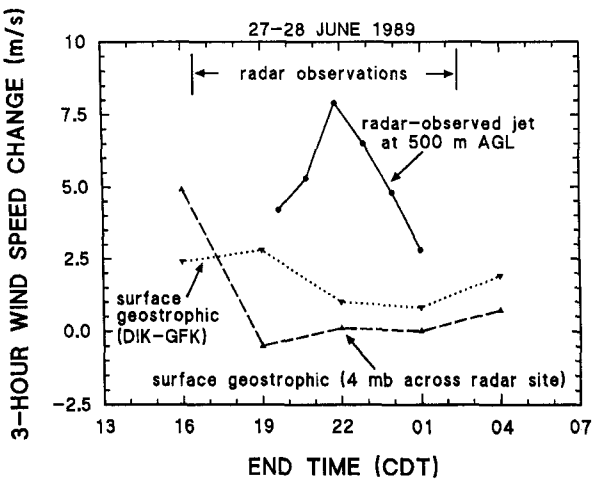

FIG. 15. Comparison of temporal changes of wind speed. Solid line shows the radar observations of wind speed measured at the level of the jet maximum. Dashed and dotted lines show the surface geostrophic values computed by two different methods (see text).

the geostrophic wind from surface-pressure maps using the spacing between the 4-mb-increment contours that most closely spanned the radar site. By either method, Fig. 15 shows that the surface geostrophic wind did not increase nearly as much as the observed acceleration of the jet. This suggests the pressure gradient force change was not the main contributor to the jet's development.

It is possible that the pressure gradient at the jet level (500 m AGL) may have increased more sharply than at the surface, and could, therefore, have accounted for a more substantial portion of the jet's speed increases. This is speculative, however, and opposite to the pressure gradient evolution near 1000 m AGL, which, based on analysis of the 850-mb maps, was weakening during most of the observational period.

Figure 15 indicates that the greatest increases of the surface geostrophic wind occurred just before the onset and during the earliest part of the radar observations. Thus, the pressure gradient force probably made its greatest impact on the jet development at this time. This may explain why, unlike in other nocturnal jet studies, the jet in this case began appearing before sunset.

A puzzling aspect of this episode concerns the vertical-velocity measurements (Fig. 8). Hourly averages from the zenith-pointing scans showed downward motions in the afternoon and upward motions at night; maximum magnitudes were almost 0.5 m s^{-1} near 0.5 km AGL. We have examined and eliminated the possibility that this could have been caused by misalignment (out of level) of the radar antenna. Therefore, we conclude this was a real feature of the airflow. There are a number of possible but not totally satisfying physical explanations.

Large-scale subsidence beneath the ridge over North Dakota may have contributed slightly to the downward motion measured in the afternoon by the radar. It is also possible that the radar was, by coincidence, located mainly below the descending motion side of a quasi-stationary boundary-layer horizontal roll circulation in the afternoon and beneath the ascending region of such a circulation at night. Vertical velocities of the observed magnitudes could easily be produced in the boundary layer by roll circulations.

The vertical motions observed by the radar are in qualitative agreement with the model results of Paegle and Rasch (1973) for a location of anticyclonic flow (such as was the case at the radar). Their nocturnal jet model, which allows for horizontal variations of geostrophic wind, predicts downward motion in the day and upward at night for this situation. While the sequence of vertical motion oscillation matches the radar observations, the maximum magnitude of the vertical wind predicted by their model is only a few centimeters per second, much less than the values the radar measured.

In analogy to circulations associated with tropopause jet streaks, convergence and divergence patterns surrounding the boundary-layer jet itself should have created vertical motions. Bonner et al. (1968) studied a boundary-layer jet over the Great Plains for which the horizontal extent and curvature of the jet was known. They showed that vertical motions of a few centimeters per second varied from rising to descending, depending on the site location with respect to the location of the jet-streak maxima. In the NDTP case, we know almost nothing about the horizontal structure of the jet, except that it was also detected at Bismarck, 50 km east of the radar. It is quite possible that the radar was located beneath a region of the jet favored for upward motion. The large magnitude of the observed rising motion, however, remains unexplained.

7. Conclusions

A single Doppler radar obtained clear-air measurements of the development of a strong boundary-layer nocturnal jet. Data from a repetitive sequence of four elevation scans were analyzed by an improved VAD method. In addition to mean wind components, the radar provided detailed measurements of the profiles of several turbulence terms. Data with a vertical resolution of about 60 m and temporal resolution of 8 min were recorded for 10 h, beginning in the late afternoon.

Boundary-layer wind speeds began to increase in the late afternoon as surface cooling began. The speeds accelerated more rapidly after sunset and eventually produced a jet that exceeded 23 m s^{-1} (1-h average) near 0.5 km AGL. Wind veered with height and time and followed the expected inertial oscillation pattern. The measured shear stresses, vertical fluxes of hori-

zontal momentum, and velocity variances, which were initially large, quickly became small after the surface began to cool. The results demonstrate the important role of the release of surface frictional restraints on the boundary-layer flow in the development of nocturnal jets. It is also probable that an increasing pressure gradient force contributed to the jet's intensification, particularly during the early part of the observation period. The directly measured vertical velocities were significantly downward during the late afternoon and upward at night when the jet was well developed.

In the past, detailed measurements of nocturnal jets have been limited to a few research episodes involving in situ sampling. The measurements shown here demonstrate the ability of Doppler radar to extend these observations. Opportunities to observe boundary-layer jets should increase greatly when operational networks of NEXRAD and wind-profiling radars are established. We hope the technique and measurements reported here will stimulate future studies of the phenomena using data from these operational remote sensors.

Acknowledgments. WPL's participation in the NDTP was sponsored by the NOAA Federal/State Cooperative Program in Atmospheric Modification Research. We are grateful to the following colleagues at WPL: Kurt Clark and Bruce Bartram for expert technical assistance in the field, Eric Moore for data processing, and Chris Fairall for helpful discussions. We also thank NDTP Coordinator Bruce Boe for the many arrangements he made for the project.

REFERENCES

Blackadar, A. K., 1957: Boundary layer wind maxima and their significance for the growth of nocturnal inversions. *Bull. Amer. Meteor. Soc.*, **38**, 283–290.

Boe, B. A., and H. L. Johnson, 1990: Destabilization antecedent to a tornadic northern High Plains mesoscale convective system: a case study. Preprints, *16th Conf. on Severe Local Storms*, Kananaskis Prov. Park, Alberta. Amer. Meteor. Soc., 538–541.

Bonner, W. D., 1966: Case study of thunderstorm activity in relation to the low level jet. *Mon. Wea. Rev.*, **94**, 167–178.

——, 1968: Climatology of the low level jet. *Mon. Wea. Rev.*, **96**, 833–850.

——, S. Esbensen, and R. Greenberg, 1968: Kinematics of the low-level jet. *J. Appl. Meteor.*, **7**, 339–347.

Browning, K. A., and R. Wexler, 1968: The determination of kinematic properties of a wind field using Doppler radar. *J. Appl. Meteor.*, **7**, 105–113.

Chadwick, R. B., and N. Hassel, 1987: Profiler: The next generation surface-based atmospheric sounding system. Preprints, *Conf. on Interactive Info. Proc. Systems for Meteorology, Oceanography, and Hydrology*, New Orleans. Amer. Meteor. Soc., 15–21.

Eberhard, W. L., R. E. Cupp, and K. R. Healy, 1989: Doppler lidar measurement of profiles of turbulence and momentum flux. *J. Atmos. Oceanic Technol.*, **6**, 809–819.

Ecklund, W. L., D. A. Carter, and B. B. Balsley, 1988: A UHF wind profiler for the boundary layer: Brief description and initial results. *J. Atmos. Oceanic Technol.*, **5**, 432–441.

Fast, J. D., and M. D. McCorcle, 1990: A two-dimensional numerical sensitivity study of the Great Plains low-level jet. *Mon. Wea. Rev.*, **118**, 151–163.

Frisch, A. S., 1991: On the measurement of second moments of turbulent wind velocity with a single Doppler radar over non-homogeneous terrain. *Bound. Layer Meteor.*, **51**, 29–39.

——, B. E. Martner, and J. S. Gibson, 1989: Measurement of the vertical flux of turbulent kinetic energy with a single Doppler radar. *Bound. Layer Meteor.*, **49**, 331–337.

Holton, J. R., 1967: The diurnal boundary layer wind oscillation above sloping terrain. *Tellus*, **19**, 199–205.

Kropfli, R. A., 1986: Single Doppler radar measurements of turbulence profiles in the convective boundary layer. *J. Atmos. Oceanic Technol.*, **3**, 305–314.

Lenschow, D. H., X. S. Li, C. J. Shu, and B. B. Stankov, 1988: The stably stratified boundary layer over the Great Plains. *Bound. Layer Meteor.*, **42**, 95–121.

Lhermitte, R. M., 1966: Probing air motion by Doppler analysis of radar clear air returns. *J. Atmos. Sci.*, **23**, 575–591.

Maddox, R. A., 1983: Large-scale meteorological conditions associated with mid-latitude mesoscale convective complexes. *Mon. Wea. Rev.*, **111**, 1475–1493.

McNider, R. T., and R. A. Pielke, 1981: Diurnal boundary layer development over sloping terrain. *J. Atmos. Sci.*, **38**, 2198–2211.

Paegle, J., and G. E. Rasch, 1973: Three-dimensional characteristics of diurnally varying boundary layer flows. *Mon. Wea. Rev.*, **101**, 746–756.

Parish, T. R., A. R. Rodi, and R. D. Clark, 1988: A case study of the summertime Great Plains low-level jet. *Mon. Wea. Rev.*, **116**, 94–105.

Raymond, D. J., 1978: Instability of the low-level jet and severe thunderstorm formation. *J. Atmos. Sci.*, **35**, 2274–2280.

Stensrud, D. J., M. H. Jain, K. W. Howard, and R. A. Maddox, 1990: Operational systems for observing the lower atmosphere: Importance of data sampling and archival procedures. *J. Atmos. Oceanic Technol.*, **7**, 930–937.

Uccellini, L. W., and D. R. Johnson, 1979: The coupling of upper and lower tropospheric jet streaks and implications for the development of severe convective storms. *Mon. Wea. Rev.*, **107**, 682–703.

Wilson, D. A., 1970: Doppler radar studies of boundary layer wind profiles and turbulence in snow conditions. *Proc., 14th Conf. on Radar Meteor.*, Tucson. Amer. Meteor. Soc., 191–196.